Purification of Yard-Glass Shaped Boron Nitride Nanotubes

Xue-Song, Lin*[+]

College of Science, Liaoning Technical University, Fuxin 123000, CHINA

Dian-Qiang, Chen

Liaoning Nonferrous Exploration and Research Institute, Shenyang 110013, CHINA

Bo, Zhong

School of Materials Science and Engineering, Harbin Institute of Technology at Weihai, Weihai, 264209, CHINA

Jian-Lin, Yang

College of Materials Science and Engineering, Liaoning Technical University, Fuxin 123000, CHINA

ABSTRACT: *An efficient method for purification of Yard-Glass Shaped Boron Nitride NanoTubes (YG-BNNTs) fabricated via a Chemical Vapour Reaction (CVR) route has been developed. Impurities including carbon, Boron Nitride (BN), and Fe species in the pristine YG-BNNT sample are removed by a combined physical and chemical procedure which involves ultrasonication, high temperature oxidation, hot-water washing and acid washing. The samples at different stages of the purification process are monitored using X-Ray powder Diffraction (XRD), X-ray Photoelectron Spectroscopy (XPS) and Transmission Electron Microscopy (TEM). The results reveal that the carbon and BN impurities could be easily eliminated. However, the catalyst nanoparticles (Fe_3C) encaged in the tubes prove to be effectively shielded from oxidation and acid corrosion. Although the content of catalyst nanoparticles could be satisfactorily reduced to about 1.0 wt% by prolonged ultrasonication and acid washing, a small number of such magnetic nanoparticles are still left in the final purified YG-BNNTs. The YG-BNNTs exhibit a typical ferromagnetic behaviour even after a longtime oxidizing and acid washing treatment, indicating that they could be potentially used for harsh-environment magnetic devices.*

KEY WORDS: *Boron nitride nanotube, Magnetic properties, Purification, Antioxidation.*

INTRODUCTION

During the past decade, Boron Nitride NanoTubes (BNNTs) have attracted considerable interests owing to their unique properties [1, 2]. BNNTs possess a superior Young's modulus and a high thermal conductivity that are comparable to Carbon NanoTubes (CNTs) [3,4]. Furthermore, BNNTs are electrical insulator and transparent to visible light due to a wide band gap (around 5.2~5.8 eV) which is almost independent of tube chirality and morphology [5,6]. In addition, BNNTs exhibit high chemical stability and resistance

* *To whom correspondence should be addressed.*

+ *E-mail: lxs488@qq.com*

1021-9986/14/1/29 *8/$/2.80*

to oxidation, which could be used as nano-scale semiconductor devices in rigorous environments [2,7]. BNNTs are deemed to be excellent candidate for composite reinforcements [8], compact laser emitters [9], protective coatings [10], hydrogen storage media [11], biological probes [12], and piezoelectric materials [13].

Many techniques including arc discharge [11], continuous laser heating or oven heating of B-containing reagent mixtures [14,15], chemical vapor deposition [16], and template confined method [17] have been developed to synthesize BNNTs. However, the yields of BNNTs are universally low compared with that of CNTs, and a number of impurities including BN, catalyst metal particles and/or amorphous carbon are commonly produced together with the BNNTs. In order to obtain the intrinsic properties of BNNTs and optimize their performances in various applications, elimination of these impurities is indispensable. A variety of purification methods, both physical and chemical, have been proposed for the purification of BNNTs. *Chen et al* [18] reported a purification technique in which the pristine sample was oxidized at high temperatures followed by acid treatment and hot-water washing. Impurities could be effectively removed by these procedures. *Vieira et al* [19] have developed a surfactant assisted filtration method resulting in highly purified BNNTs. According to *Zhi et al* [20], BNNTs could be purified by a polymer wrapping and filtration route. In these studies, the pristine BNNTs used are mainly cylindrical BNNTs or bamboo shaped BNNTs, where the catalyst particles are rarely encased in the tubes and are relatively easy to remove. Recently, another type of BNNTs, the so-called Yard-Glass shaped BNNTs (YG-BNNTs), has been fabricated [15]. Metal catalyst nanoparticles are mostly encapsulated in the tubes, which makes them impervious to acid dissolution. Purification of the YG-BNNTs appears to be a technical challenge and, to the best of our knowledge, has not been reported so far.

In this study, we present a multistep purification method to remove most of the foreign substances in the pristine YG-BNNT samples, including the metal particles encased in the tubes, the carbon and BN impurities. The method developed here is similar to that proposed by *Chen et al* [18] with the differences that ultrasonication is conducted prior to high temperature oxidation, and that the temperatures used during the oxidation process are higher in order to eliminate BN impurity effectively. The protection effects of the BN walls on the catalyst nanoparticles are discussed and the magnetic properties of the purified YG-BNNTs are also evaluated.

EXPERIMENTSAL SECTION

The starting pristine YG-BNNT samples were synthesized by a chemical vapour reaction method at 1450 °C under N_2 pressure (1.8 MPa). A mixture of 6.0 g Ammonia Borane (AB) and 1.5 g ferrocene was used as precursor. AB was synthesized according to the method proposed by *Ramachandran et al* [21]. A 30 L graphite crucible lined with filter papers was used as a reactor. White YG-BNNTs were obtained on the graphitized filter papers after 2 h annealing. Fig. 1(a) and (b) display the SEM and TEM images of the as-grown YG-BNNTs, respectively. It is evident that catalyst nanoparticles are encaged in the knobs of the tubes. Combined SEM, EDX and TEM analysis (not shown here) indicates that the catalyst nanoparticles in the tubes are Fe_3C and other impurities including carbon, BN and Fe-containing species (Fe simple substance and FeB_x) are present on the substrates under the YG-BNNT layer. These are the primary impurities to be removed in this study.

The purification procedure is schematically shown in Fig. 2. Firstly, 4.0 g raw materials containing both YG-BNNTs and the substrates were ultrasonicated in 200 mL ethanol for about 20 min. The YG-BNNTs were peeled off from the substrates and suspended in the ethanol. Nearly 500 mg YG-BNNTs with small quantities of impurities were obtained by filtrating the suspension. A typical SEM image of the ultrasonicated sample is depicted in Fig. 1(c), which clearly shows that some tiny fragments of substrate are present in the sample (as indicated by the white arrow) and the YG-BNNTs are broken into short segments by ultrasonication. To further purify the samples, a high temperature oxidation treatment (850 °C for 4 h) was carried out to remove the carbon impurity and simultaneously convert the BN impurity into amorphous B_2O_3. Subsequently, the sample was washed by hot water (98 °C) to eliminate the amorphous B_2O_3. The resultant product was then leached in a concentrated HCl solution (6 M) at 70 °C for 15 h. The green colour observed in the HCl solution provides an indication that the Fe-containing impurities were removed during this process. The final step was to collect the leached sample by washing and filtration.

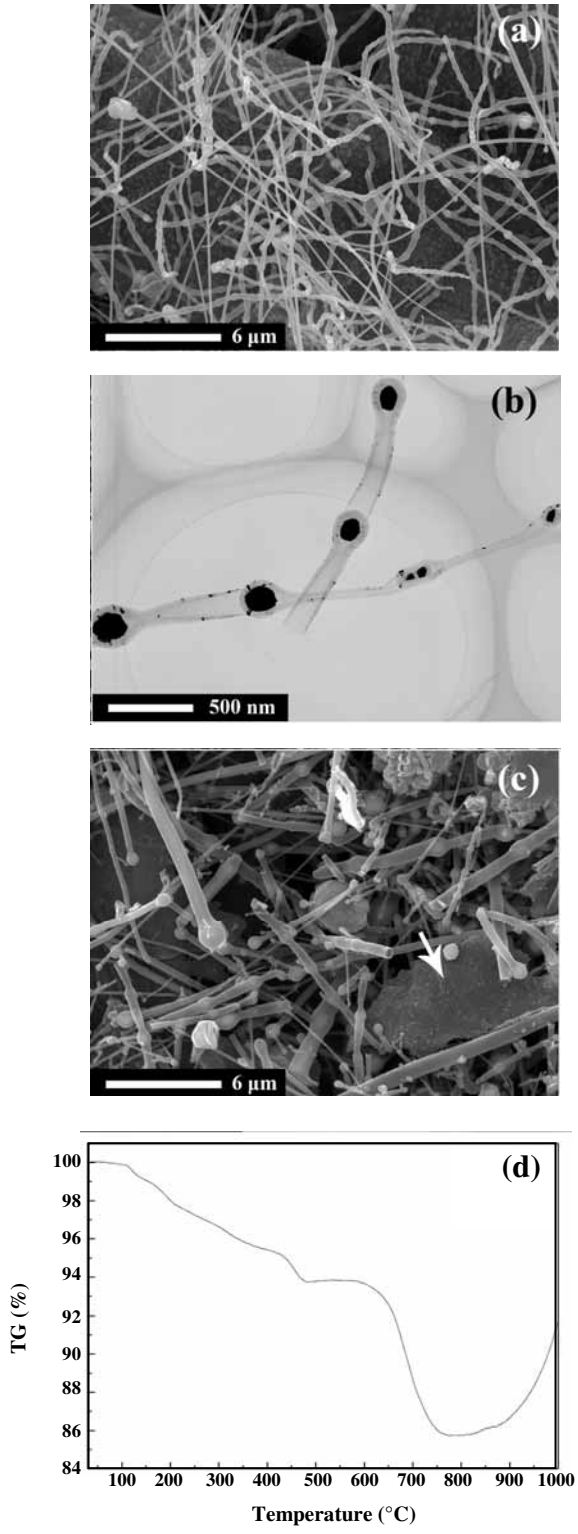

Fig. 1: (a) SEM and (b) TEM images of the as-grown YG-BNNTs. (c) SEM image of the ultrasonicated YG-BNNTs. (d) TG curve of the ultrasonicated sample at a heating rate of 10 °C / min in air.

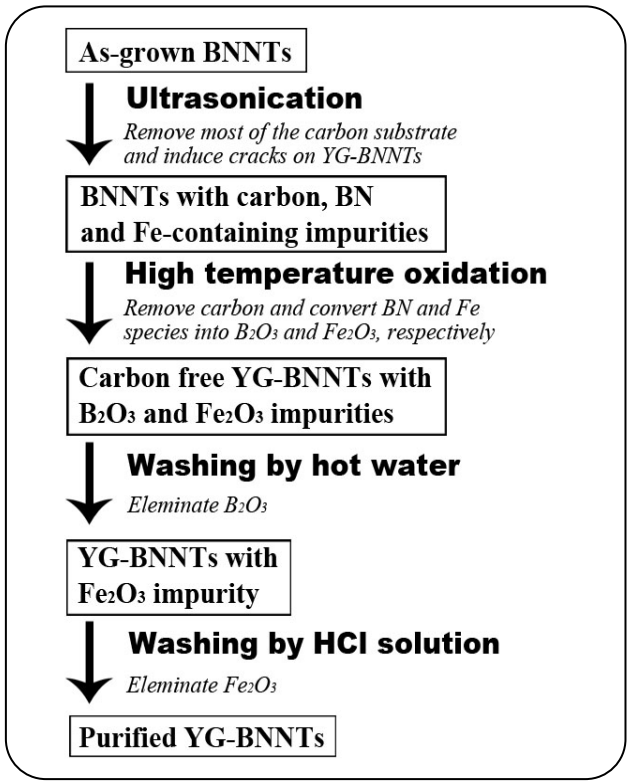

Fig. 2: Flow chart of the purification procedure.

The YG-BNNT samples at different purification stages were characterized by Scanning Electron Microscopy (SEM, MX2600EF equipped with Energy Dispersive X-ray (EDX)spectroscopy), Transmission Electron Microscopy (TEM, Philips TECNAI 20), Thermo-Gravimetric Analyzer (TGA, Netzsch STA449C), X-Ray powder Diffraction (XRD, Rigaku D/max-γB X-ray diffractometer with Cu K radiation (λ=0.154178nm)), and X-ray Photoelectron Spectroscopy (XPS, PHI 5700 ESCA System with a PC-ACCESS data analysis system (Physical Electronics Inc.)). The room temperature magnetization was measured by vibrating sample magnetometer (VSM, Lake Shore 7410).

RESULTS AND DISCUSSIONS

High temperature oxidation

High temperature oxidation treatment is a crucial step of the purification process. For one thing, carbon impurity could be removed by the oxidation. For another, BN impurity rather than YG-BNNTs could be converted to amorphous B_2O_3 at a controlled temperature because BNNTs are more oxidation resistant (BNNTs can withstand up to 900-1000 °C in air [20]) and the resultant B_2O_3 could be easily eliminated by hot-water washing.

To achieve an optimum oxidizing temperature, TG analysis was first conducted on the ultrasonicated sample. The sample was heated up to 1000 °C at a rate of 10 °C min^{-1} in air and the weight changes as a function of heating temperature is shown in Fig. 1(d). A sharp weight loss around 700 °C corresponds to the rapid carbon oxidation. The slow weight increase from 800 to 900 °C indicates the oxidization of BN and Fe-containing impurities. The rapid weight increase above 900 °C is ascribed to the oxidation of the YG-BNNTs. Based on the TG analysis, 800~850 °C seems an appropriate temperature interval that can eliminate the carbon impurity and convert the BN impurity to B_2O_3 while keeping YG-BNNTs unaffected.

The XRD pattern of the ultrasonicated sample is shown in Fig. 3(a), from which four crystalline phases could be indexed: hexagonal BN (JCPDS 34-0421), α-Fe (JCPDS 06-0696), Fe_3C (JCPDS 35-0772) and carbon (JCPDS 46-0943). This unambiguously indicates the impurities that exist in the samples. It is noteworthy that the BN phase not only originates from the YG-BNNTs, but also comes from the impurity BN. To further determine the optimal oxidation temperature, the ultrasonicated samples were oxidized in air for 4 h at 800 and 850 °C, respectively. The corresponding XRD patterns are shown in Fig. 3(b) and (c). A new Fe_2O_3 phase (JCPDS 33-0664) could be identified from these two patterns and its peak intensities are much stronger in Fig. 3(c). This suggests that the Fe-containing impurities on the substrates are intensively oxidized at the elevated temperatures but the levels of oxidations are distinct. Fe-containing impurities are oxidized more thoroughly at 850 °C. Carbon phase evidenced in pristine sample is absent after oxidation at 800 °C, indicating the carbon impurity has been completely removed. This is also supported by EDX analysis. A typical EDX spectrum taken from the sample oxidized at 800 °C is shown in Fig. 4(a), clearly indicating the absence of carbon. Another notable feature in Fig. 3(b) and (c) is that an amorphous phase appears after 850 °C oxidation, which implies the conversion of the BN impurity to the amorphous B_2O_3. Although the carbon impurity could be easily removed at 800 °C, it seems that BN impurity has not been completely oxidized at 800 °C and the optimum oxidation temperature that could thoroughly converts the BN impurity to amorphous B_2O_3 should be higher.

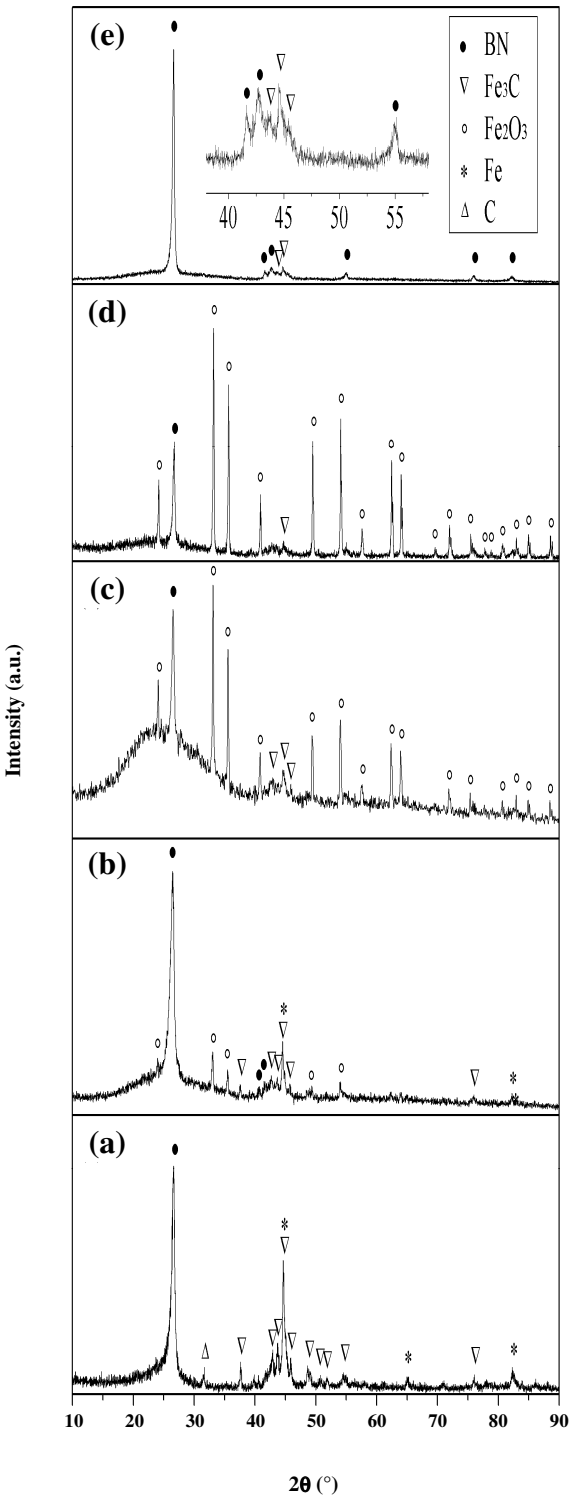

Fig. 3: XRD patterns of YG-BNNTs samples (a) right after ultrasonication, (b) oxidized at 800 °C for 4 h, (c) oxidized at 850 °C for 4 h, (d) after hot-water washing, and (e) after acid washing.

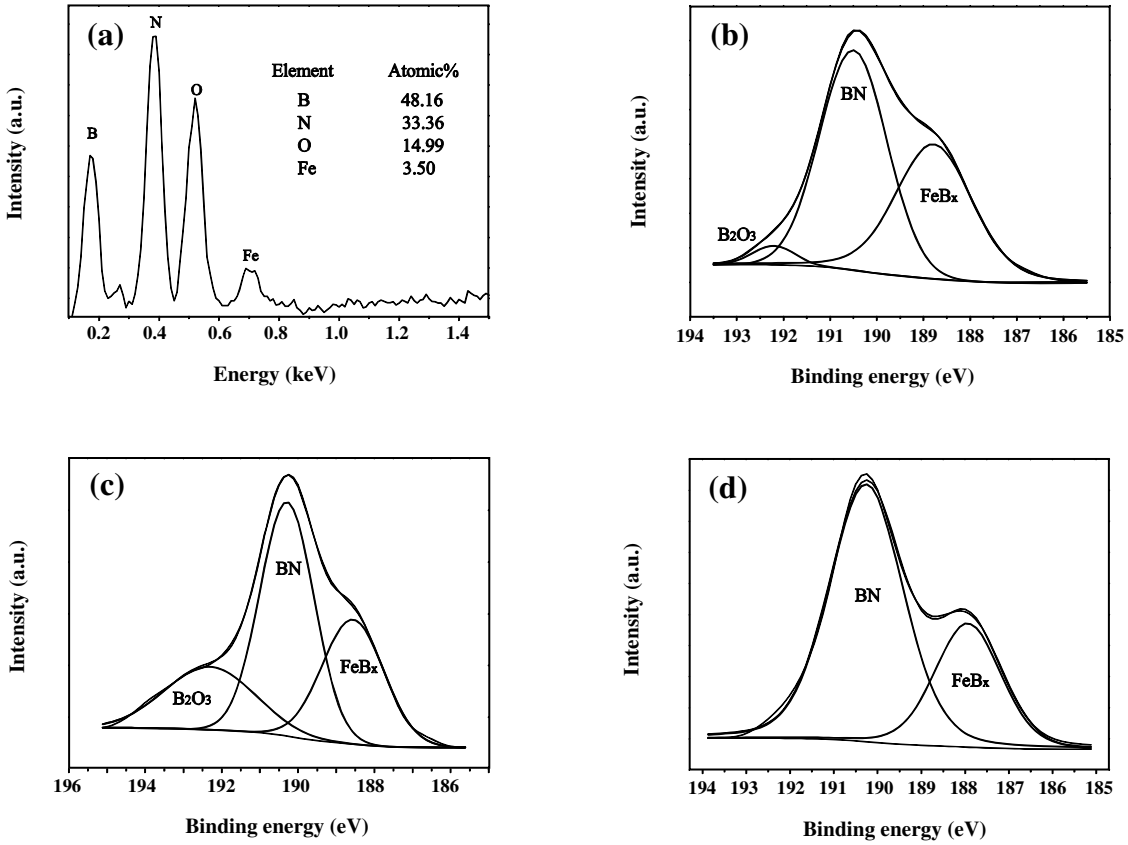

Fig. 4: (a) EDX spectrum of the 800 °C oxidized sample. B1s XPS spectra recorded from the samples (b) after oxidation at 800 °C, (c) after oxidation at 850 °C and (d) after hot-water washing.

It is worth noting that the Fe_3C nanoparticles encapsulated in the BNNTs are protected from oxidation by the BN walls during the oxidizing process, as indicated by the diffraction peaks of Fe_3C phase in both patterns.

XPS analysis was performed to further assess the chemical composition of the oxidized samples. Fig. 4(b) and (c) depict the B1s spectra recorded from the samples oxidized at 800 °C and 850 °C, respectively. Both of the broad B1s band can be decomposed into three Gaussian components. The more intense component around 190.5 eV is assigned to boron atoms surrounded only by nitrogen atoms, similar to that occurring in pure hexagonal boron nitride [22], while the component around 192.4 eV is attributed to boron atoms in B_2O_3 [23] because the oxygen atoms are more electronegative than nitrogen atoms and tend to shift the binding energy of the B atoms upwards. Another component around 188.5 eV can be ascribed to FeB_x [23] which probably arises from the reaction between BN and Fe species on the tiny fragments of the substrate during the oxidation process. XPS analysis suggests that the B_2O_3 contents in the two samples are notably different. Heating at 850 °C could convert the BN impurity to amorphous B_2O_3 more completely than at 800 °C and achieve selective oxidation of most BN impurity while keeping the structures of YG-BNNTs unchanged, which is consistent with the XRD results. Therefore, 850 °C was selected as the optimal oxidation temperature and the sample oxidized at 850 °C was used in the subsequent purification steps.

Elimination of amorphous B_2O_3 and Fe-containing impurities

Carbon impurity has been removed by the high temperature oxidation, which was accompanied by a conversion of the BN and Fe-containing impurities to amorphous B_2O_3 and Fe_2O_3, respectively. B_2O_3 could be easily eliminated by hot-water washing. XRD analysis on the hot-water washed sample as shown in Fig. 3(d) no longer detects the amorphous B_2O_3. Fig. 4(d) depicts

the B1s XPS spectrum of the hot-water washed sample. The B_2O_3 peak around 192.5 eV is negligible. These results suggest that the amorphous B_2O_3 (and thus the BN impurity) has been effectively removed by hot-water washing. The following step is to eliminate the Fe_2O_3 by acid washing, which would result in the final purified YG-BNNTs. XRD pattern of the final sample is shown in Fig. 3(e). The dominant BN phase indicates that the final sample is primarily composed of YG-BNNTs and the impurities are nearly completely removed. The method proposed in this study proves satisfactory for the purification of YG-BNNTs.

It is noted, however, that apart from the predominant BN peaks, a few minor phase peaks could also be identified from the XRD pattern of the final sample (see inset of Fig. 3(e)). These peaks could be indexed to the orthorhombic Fe_3C phase, which arises from the catalyst nanoparticles encapsulated in the knobs of the YG-BNNTs. This suggests that although the YG-BNNTs have undergone a high temperature oxidation at 850 °C for 4 h and a concentrated acid solution corrosion for 15 h, some of the Fe_3C nanoparticles encased in the tubes were still not oxidized or dissolved owing to the protection of the BN walls. In order to verify the existence of the catalyst nanoparticles in the purified samples, TEM analysis was carried out. It is demonstrated that although most of the nanoparticles encaged in the YG-BNNTs have been removed by the acid washing treatment, some nanoparticles could occasionally be found, as shown in Fig. 5. A notable feature is that the nanoparticles protected from oxidation and acid corrosion are all sealed in the Yard-Glass (YG) units, while the nanoparticles in open YG units are wholly missing. This indicates that the integrity of the YG units is essential to the protection effect. As stated above, ultrasonic treatment could open the ends of the YG units by cutting the tubes into segments or induce cracks on the joints of the YG units. Therefore, the oxygen or acid cations could access into the tubes through these defects during the purification process and react with Fe_3C nanoparticles, which results in their removal. This suggests that the ultrasonication facilitates the access of the oxygen and acid reagents into the tubes and is responsible for the elimination of the nanoparticles.

The protection effects of the BN walls on the Fe_3C nanoparticles have been evidenced during the purification process. Although the YG-BNNTs could be satisfactorily purified, prolonged ultrasonication and acid washing are expected to be beneficial for thorough elimination of the Fe_3C nanoparticles encased in the tubes and may further improve the purity of the final sample.

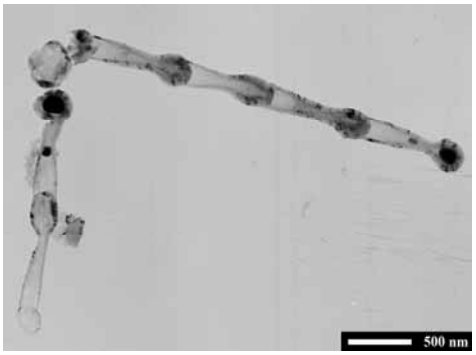

Fig. 5: TEM image of an individual YG-BNNT after purification showing that a small number of the nanoparticles are effectively protected by BN walls.

Magnetic properties of YG-BNNTs after acid treatment

Magnetic nanoparticles exhibit a number of excellent attributes that make them indispensible in a wide range of applications. Magnetic nanoparticles with various compositions have been successfully fabricated, but an unavoidable challenge is their intrinsic instability. Such particles tend to aggregate and are easily oxidized or/and corroded in air, which normally results in degradation of magnetism [24]. Therefore, it is of significance to develop protection strategies to stabilize these nanoparticles.

It seems that the Fe_3C nanoparticles encased in the BNNTs are natural magnetic nanoparticles that have been protected by the outer BN walls against the oxidation and acid corrosion. Furthermore, the nearly uniform distribution of the nanoparticles in the tubes spontaneously guarantees an excellent dispersibility that resists aggregation. Inspired by these interesting features, we performed the VSM measurement on the final YG-BNNT sample to investigate their magnetic properties. A magnetic hysteresis loop of the BNNT protected magnetic nanoparticles is shown in Fig. 6. The value of the saturation magnetization Ms is 1.3565 emu / g, which is much smaller than that of the bulk Fe_3C (~130 emu / g) [2]. This is attributed to the reduction of Fe_3C nanoparticle concentration and the formation of a surface shell with

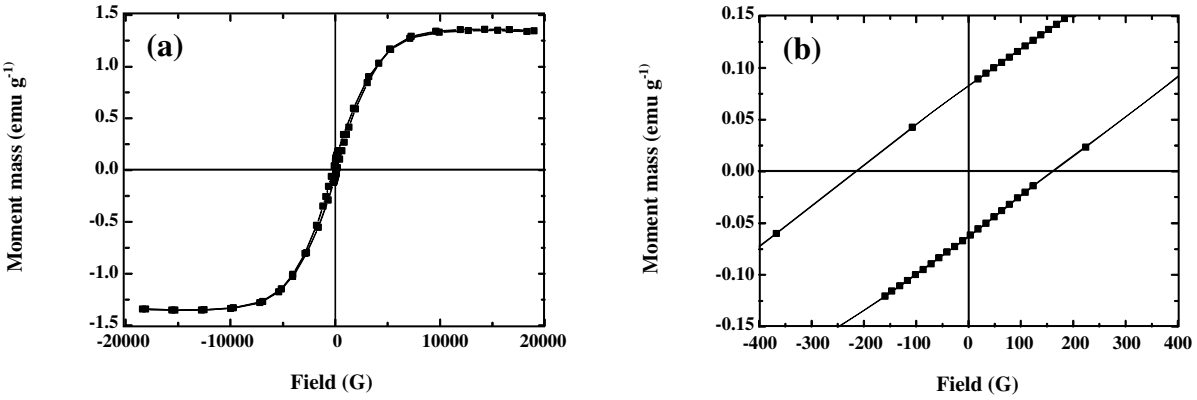

Fig. 6: Hysteresis loop of YG-BNNTs after acid treatment. (a) Full hysteresis loop, (b) An enlarged section of the hysteresis loop.

spin disorder in the purified YG-BNNT sample [15, 26]. The Fe_3C content of the purified YG-BNNTs could be estimated from the ratio of the saturation magnetization of purified sample to that of the bulk Fe_3C, i.e. 1.3565 / 130 ≈ 1 wt%. The values of remanence Mr and coercivity Hc are 0.073 emu g^{-1} and ~187.96 G, respectively. The superparamagnetic effect that is normally found in magnetic nanoparticles is not observed in our samples. This is ascribed to the relatively larger diameters of our Fe_3C nanoparticles (20~400 nm). nanoparticles above a critical value (typically 10~20 nm) would not exhibit surperparamagnetic property due to the presence of domain walls [24]. It is evident that the purified YG-BNNTs still exhibit a typical ferromagnetic behaviour even after a longtime oxidizing and acid washing treatment. Therefore, the magnetic properties of the Fe_3C nanoparticles are confirmed to be protected by the BN walls and thus the YG-BNNTs could be potentially used in harsh environments as nano-scaled magnetic devices [15].

CONCLUSIONS

In summary, we have developed a purification method to remove most of the impurities in pristine YG-BNNT samples. Carbon and BN impurities could be easily eliminated by high temperature oxidation followed by hot-water washing. The protection effect of the BN walls on the nanoparticles encapsulated in the tubes is confirmed. Longtime ultrasonication and acid washing are applied to remove the Fe_3C nanoparticles, achieving a satisfactorily purified YG-BNNT sample with a low Fe_3C content (about 1.0 wt%). The YG-BNNTs with magnetic nanoparticles protected by BNNTs exhibit a typical ferromagnetic behaviour even after the high temperature oxidation and acid washing treatments. They have great potential to be used as nano-scale magnetic materials working in rigorous environments. Although this method is based on the YG-BNNT samples fabricated using the chemical vapour reaction method, it can be generalized to purify YG-BNNT samples containing similar impurities prepared by other methods.

Received : Apr. 14, 2013 ; Accepted : Dec. 2, 2013

REFERENCES

[1] Chopra N.G., Luyken R.J., Cherrey K., Crespi V.H., Cohen M.L., Louie S.G., Zettl A., Boron Nitride Nanotubes. *Science*, **269** p. 966 (1995).

[2] Golberg D., Bando Y., Tang C., Zhi C., . Boron Nitride Nanotubes. *Adv. Mater*. **19**, p. 2413 (2007).

[3] Suryavanshi A.P., Yu M.F., Wen J., Tang C., Bando Y., Elastic Modulus and Resonance Behavior of Boron Nitride Nanotubes, *App. Phys. Lett.*, **84**, p. 2527 (2004).

[4] Chang C W, Fennimore A M, Afanasiev A, Okawa D, Ikuno T, Garcia H, Li D, Majumdar A, Zettl A., Isotope Effect on the Thermal Conductivity of Boron Nitride Nanotubes. *Phys. Rev. Lett*., **97,** 085901-1-4 (2006).

[5] Zhi C, Bando Y, Tang C, Xie R, Sekiguchi T and Golberg D., Perfectly Dissolved Boron Nitride Nanotubes Due to Polymer Wrapping. *J. Am. Chem. Soc.*, **127** , p. 15996 (2005).

[6] Blase X, Rubio A, Louie S G and Cohen M.L., Stability and Band Gap Constancy of Boron Nitride Nanotubes, *Europhys. Lett.*, **28**, p. 335 (1994).

[7] Tang C., Bando Y., Effect of BN Coatings on Oxidation Resistance and Field Emission of SiC Nanowires*, Appl. Phys. Lett.*, **83**, p. 659 (2003).

[8] Zhi C., Bando Y., Terao T., Tang C., Kuwahara H., Golberg D., Towards Thermoconductive, Electrically Insulating Polymeric Composites with Boron Nitride Nanotubes as Fillers. *Adv. Funct. Mater.,* **19**, p. 1857 (2009).

[9] Arenal R Peňa F., Stéphan O., Walls M., Tencé M., Loiseau A., Colliex C., Extending the Analysis of EELS Spectrum-imaging Data, from Elemental to Bond Mapping in Complex Nanostructures, *Ultramicroscopy,* **109**, p.32 (2008).

[10] Li Y., Dorozhkin P.S., Bando Y., Golberg D., Controllable Modification of SiC Nanowires Encapsulated in BN Nanotubes. *Adv. Mater.,* **17**, p. 545 (2005).

[11] Mpourmpakis G., Froudakis G.E., Why Boron Nitride Nanotubes are Preferable to Carbon Nanotubes for Hydrogen Storage? An ab Initio Theoretical Study, *Catal. Today,* **120**, p. 341 (2007).

[12] Chen X., Wu P., Rousseas M., Okawa D., Gartner Z., Zettl A., Bertozzi C.R., Boron Nitride Nanotubes Are Noncytotoxic and Can Be Functionalized for Interaction with Proteins and Cells, *J. Am. Chem. Soc.*, **131**, p. 890 (2009).

[13] Bai X., Golberg D., Bando Y., Zhi C., Tang C., Mitome M., Kurashima K., Deformation-Driven Electrical Transport of Individual Boron Nitride Nanotubes, *Nano Lett.*, **7**, p. 632 (2007).

[14] Arenal R., Stephan O., Cochon J., Loiseau A., Root-Growth Mechanism for Single-Walled Boron Nitride Nanotubes in Laser Vaporization Technique, *J. Am. Chem. Soc.*, **129**, p. 16183 (2007).

[15] Chen Z.G., Zou J., Li F., Liu G., Tang D.M., Li D., Liu C., Ma X., Cheng H.M., Lu G.Q., Zhang Z., Growth of Magnetic Yard-Glass Shaped Boron Nitride Nanotubes with Periodic Iron Nanoparticles, *Adv. Funct. Mater.*, **17**, p. 3371 (2007).

[16] Guo L., Singh R.N., Selective Growth of Boron Nitride Nanotubes by Pplasma-Enhanced Chemical Vapor Deposition at Low Substrate Temperature, *Nanotechnology*, **19**, p. 065601 (2008).

[17] Bechelany M., Bernard S., Brioude A., Cornu D., Stadelmann P., Charcosset C., Fiaty K., Miele P., Synthesis of Boron Nitride Nanotubes by a Template-Assisted Polymer Thermolysis Process, *J. Phys. Chem.,* C **111**, p. 13378 (2007).

[18] Chen H., Chen Y., Yu J., Williams J.S., Purification of Boron Nitride Nanotubes, *Chem. Phys. Lett.*, **425**, p. 315 (2006).

[19] Vieira S.M.C., Carroll D.L., Purification of Boron Nitride Multiwalled Nanotubes, *J. Nanosci. Nanotechnol.*, **7**, p. 3318 (2007).

[20] Zhi C., Bando Y., Tang C., Honda S., Sato K., Kuwahara H., Golberg D., Purification of Boron Nitride Nanotubes through Polymer Wrapping, *J. Phys. Chem.,* B **110**, p. 1525 (2006).

[21] Ramachandran P.V., Gagare P.D., Preparation of Ammonia Borane in High Yield and Purity, Methanolysis, and Regeneration, *Inorg. Chem.*, **46**, p. 7810 (2007).

[22] Guimon C., Gonbeau D., Pfister-Guillouzo G., Dugne O., Guette A., Naslain R., Lahaye M., XPS Study of BN Thin Films Deposited by CVD on Sic Plane Substrates, *Surf. Interface Anal.*, **16**, p. 440 (1990).

[23] Moulder J.F., Stickle W.F., Sobol P.E., Bomben K.D., Handbook of X-Ray Photoelectron Spectroscopy (Eden Prairie, MN: Perkin-Elmer Corporation) pp. 38-39 (1992).

[24] Lu A.H., Salabas E.L., Schüth F., Magnetic Nanoparticles: Synthesis, Protection, Functionalization, and Application. *Angew. Chem. Int. Ed.*, **46**, p. 1222 (2007).

[25] David B., Schneeweiss O., Mashlan M., Šantavá E., Morjan I., Low-Temperature Magnetic Properties of Fe_3C/Iron Oxide Nanocomposite, *J. Magn. Magn. Mater.*, **316**, p. 422 (2007).

[26] Sajitha E.P., Prasad V., Subramanyam S.V., Mishra A.K., Sarkar S., Bansal C., Size-Dependent Magnetic Properties of Iron Carbide Nanoparticles Embedded in a Carbon Matrix, *J. Phys.: Condens. Matter*, **19**, p. 046214 (2007).